A new view of the Spiral Structure of the Northern Outer Milky Way in Carbon Monoxide

Yan Sun,[1] Ji Yang,[1] Shaobo Zhang,[1] Qing-Zeng Yan,[1] Yang Su,[1] Xuepeng Chen,[1] Xin Zhou,[1] Ye Xu,[1] Hongchi Wang,[1] Min Wang,[1] Zhibo Jiang,[1] Ji-Xian Sun,[1] Deng-Rong Lu,[1] Bing-Gang Ju,[1] Xu-Guo Zhang,[1] and Min Wang[1]

[1]*Purple Mountain Observatory, Chinese Academy of Sciences, Nanjing 210008, China*

ABSTRACT

Based on 32,162 molecular clouds from the Milky Way Imaging Scroll Painting project, we obtain new face-on molecular gas maps of the northern outer Galaxy. The total molecular gas surface density map reveals three segments of spirals, extending 16–43 kiloparsecs in length. The Perseus and Outer arms stand out prominently, appearing as quasi-continuous structures along most of their length. At the Galactic outskirts, about 1,306 clouds connect the two segments of the new spiral arm discovered by Dame & Thaddeus (2011) in the first quadrant and Sun et al. (2015) in the second quadrant, possibly extending the arm into the outer third quadrant. Logarithmic spirals can be fitted to the CO arm segments with pitch angles ranging from 4° to 12°. These CO arms extend beyond previous CO studies and the optical radius, reaching a galactic radius of about 22 kiloparsecs, comparable to the Hɪ radial range.

1. INTRODUCTION

Spiral galaxies have long captivated astronomers with their striking spiral structures, characterized by active star formation and dense interstellar medium (ISM). Among them, the Milky Way has been proposed as a spiral galaxy for centuries (Alexander 1852), but its observed spiral patterns remain uncertain (e.g., Benjamin 2009; Dobbs & Baba 2014; Xu et al. 2018). The challenge primarily stems from our position deep within the galactic disk, where the presence of abundant interstellar dust renders optical studies ineffective beyond several kiloparsecs (e.g., Levine et al. 2006). Radio wavelength observations, particularly the Hɪ and CO line emissions, offer a promising avenue for exploring of the gaseous disk extending far beyond the stellar disk (e.g., Kerr 1969; Braine & Herpin 2004; Kalberla & Kerp 2009; Heyer & Dame 2015).

Corresponding author: Yan Sun & Ji Yang
yansun@pmo.ac.cn, jiyang@pmo.ac.cn

Since its initial discovery, the intense Hɪ 21-cm line emission originating from the atomic phase of the ISM has shown quasi-continuous features in longitude-velocity space, commonly interpreted as spiral arms (e.g., Weaver 1974). Hɪ has provided a comprehensive view of the Galactic disk (e.g., Kerr et al. 1957; Burton 1971; Strasser et al. 2007; Mertsch & Phan 2023). However, despite its utility, the Hɪ spiral structure is still unclear or blurry in the total Hɪ surface density map (e.g., Levine et al. 2006; Kalberla & Kerp 2009). A critical issue is the large intrinsic velocity dispersion, which causes features to be smeared along the line of sight by confusing the velocity-distance transformation (Kalberla & Kerp 2009). Additionally, Hɪ contains both cold- and warm-phase (a few thousand K) gases and can extend even beyond the disk to the starless disk-halo interface (McClure-Griffiths et al. 2023), which further complicates its role as an ideal arm tracer. To address these issues, various methods have been developed, such as transforming line flux within narrow velocity intervals (e.g., Kerr 1969; Koo et al. 2017), or applying unsharp masking techniques to enhance the visibility of spiral structures (Levine et al. 2006). De-
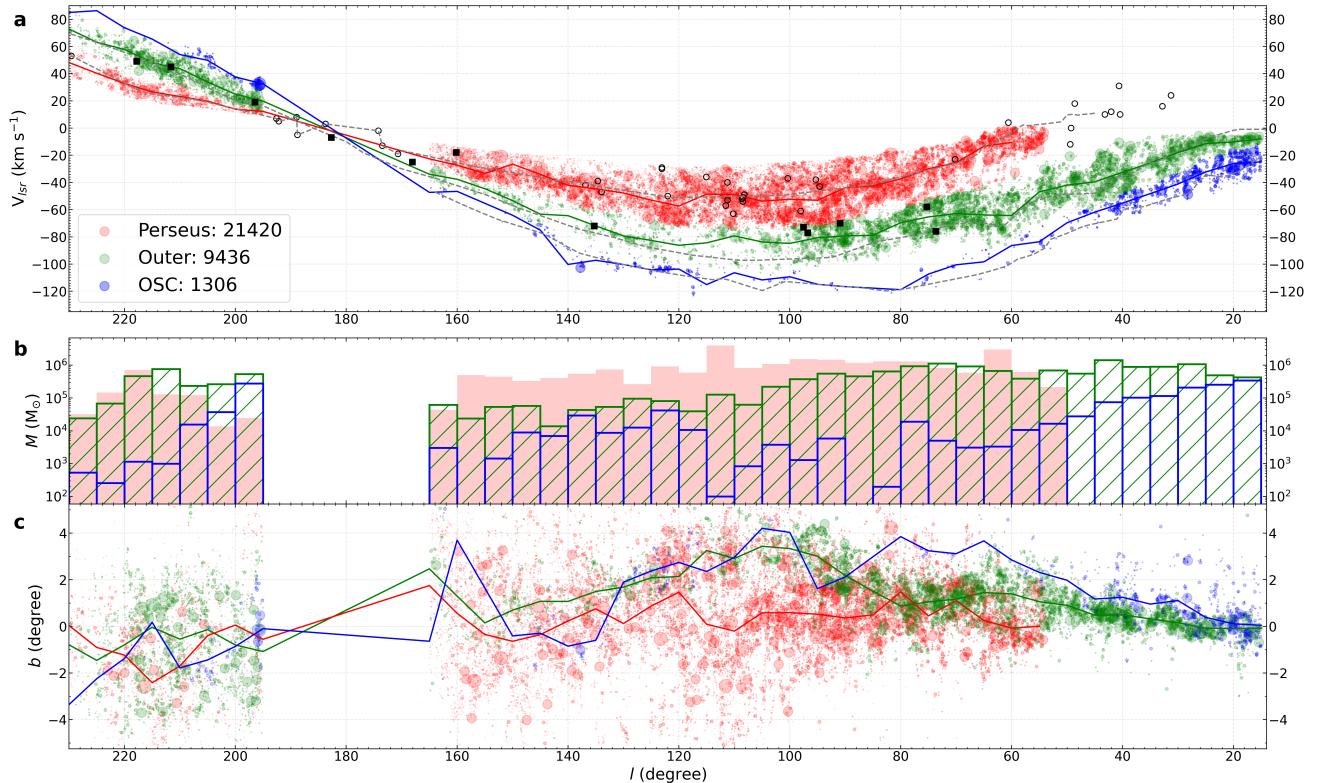
Figure 1. (*a*) Molecular cloud distribution in the l-v_{lsr} map. The total numbers of MCs in each spiral arm are indicated in the corner. The size of individual circles gives an indication of cloud mass. The smallest circle is related to molecular clouds with a mass less than 100 $M_\odot$, while the largest circle corresponds to those with a mass greater than 10^6 $M_\odot$. The grey and color-coded lines represent the spiral-arm loci from Reid et al. (2019) and MCs in this study. (*b*) Histograms illustrate the mass distributions of each spiral arm along the Galactic longitude in each $5°$ bin. (*c*) Distribution of MCs in the Galactic coordinates (l, b). The HMSFRs of the Perseus and Outer arm segments are indicated by open circles and filled squares, respectively (Reid et al. 2019).

spite these efforts, discrepancies persist among studies even when utilizing the same observational data.

In contrast, as it traces the cold and dense component of the ISM and is closely related to star formation, CO line emission offers a more conventional arm indicator. Furthermore, owing to its small velocity dispersion, the CO emission can be well defined as a series of discrete molecular clouds (MCs), which can serve as an alternative way to construct the face-on spiral structure from the central velocity of each MC, in addition to directly constructing it from the velocity of each voxel in the (position-position-velocity) PPV cube. Therefore, CO molecular clouds are expected to delineate compelling spiral structures across the entire disk. However, limited by the combined effects of the much reduced intensity of the CO line and the sensitivity of previous CO surveys, the global CO spiral structures were determined within a much smaller Galactic range than H I (Pohl et al. 2008; Nakanishi & Sofue 2016; Rice et al. 2016; Miville-Deschênes et al. 2017; Mertsch & Vittino 2021). As a result, much of the outer Galactic molecular

disk remains largely unexplored (as recently reviewed by Watson & Koda 2017).

The new deeper CO survey–Milky Way Imaging Scroll Painting (MWISP; Su et al. 2019; Sun et al. 2021) conducted with the PMO 13.7-m millimeter-wavelength telescope (Yang et al. 2008; Shan et al. 2012; Sun et al. 2018a), offers us a unique opportunity to uncover the distant large-scale molecular structures. In more recent years, some progress on large-scale molecular structures has been made based on MWISP's early data, i.e., the identification of the new segment of the distant spiral arm (Sun et al. 2015, 2017), and the apparent reveal of the Outer arm in the form of molecular gas (Su et al. 2016; Du et al. 2016; Dong et al. 2023) in the regions of $l=[35°, 45°]$, $[100°, 150°]$ and $[220°, 230°]$. Currently, the MWISP survey has fully covered the Galactic coordinate ranges of $l=[12°, 230°]$ and $b=[-5.25°, 5.25°]$. Using this dataset, we focus on the face-on spiral structures in the outer Galaxy, where velocity crowding is alleviated, and distances can be unambiguously estimated from the observed radial velocity. Although the Local
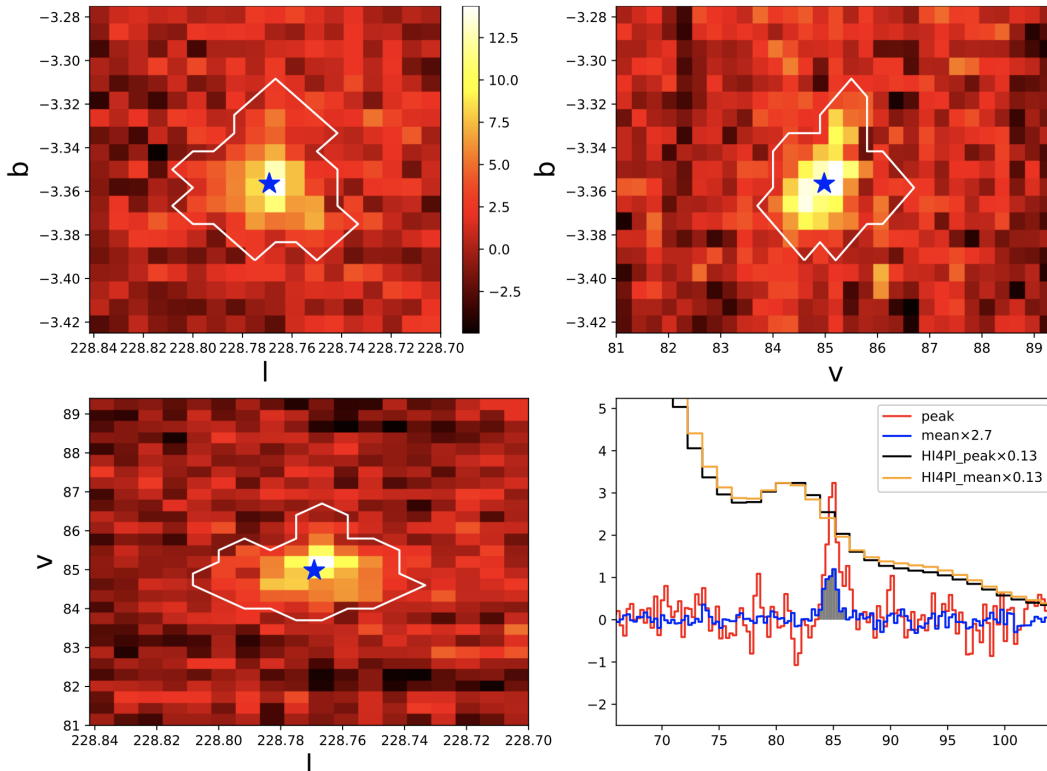
Figure 2. An example of molecular clouds probably lying along the new extension of the OSC arm in the third quadrant. The blue stars indicate the center of the cloud. The white contours indicate the boundary of the cloud in the *l-b-v* intensity maps. The CO and H I spectra show emission at the CO emission peak and emission averaged over the white boundary.

arm is part of the Outer Galaxy, it is excluded from the scope of this study due to its broad distribution in Galactic latitude, which is not well covered by current MWISP data, as well as the significant uncertainty in its kinematic distance.

2. MOLECULAR CLOUDS DISTRIBUTION IN THE (L, B, v_{lsr}) SPACE

We use so far the largest sample comprising 32,162 MCs, which were generated using a density-based spatial clustering of applications with the noise (DBSCAN, Es-ter et al. 1996; Yan et al. 2020) algorithm applied to the MWISP data. The algorithm can effectively identifies contiguous PPV voxels above a given intensity thresh-old and has been tested against other widely used al-gorithms by Yan et al. (2022). DBSCAN, like other algorithms, faces limitations in crowded regions where it may mistakenly group unrelated structures into a sin-gle cloud or, in areas with low sensitivity, split emis-sions that belong to the same cloud into different clouds. These are common uncertainties encountered when ex-tracting individual clouds from PPV data cubes. How-ever, this issue is largely mitigated in the lower cloud density outer Galaxy. The sample has been filtered by visual inspection of the morphology and spectra of each MC. Therefore, the MCs of this sample represent the

confident ones. More details regarding the identifica-tion and properties of these MCs are presented in Sun et al. (accepted by ApJS, 2024, hereafter Paper I).

Figure 1 presents the distributions of these 32,162 MCs in the Galactic coordinates. Each MC was assigned to a spiral arm by matching its Galactic longitude and LSR velocity to the nearest known spiral arm on the *l-*v_{lsr} map (see the grey-dashed lines in Fig. 1), which is primarily based on CO, H I, or maser data (Reid et al. 2019). This method assumes that the boundaries of each spiral arm are defined by equal velocity separations from the centers of adjacent arms. The total number of MCs assigned to the three spiral arm segments is also indi-cated in Fig. 1.

The MCs along the outermost feature over a longitude range of 15°-165° (Fig. 1a) confirm our previous hypoth-esis that the OSC arm might extend into the outer sec-ond quadrant (Sun et al. 2015). Most surprisingly, how-ever, is that a feature at the largest positive velocity might be a new extension of the OSC arm, from $(l, b, v) \approx (195°, -1.2°, 36\,\mathrm{km\,s^{-1}})$, to $(230°, -3°, 83\,\mathrm{km\,s^{-1}})$, running roughly parallel to the locus of the Outer arm but shifted by $\sim 15\,\mathrm{km\,s^{-1}}$ to more positive velocities. The shifting is much larger than the typical cloud-cloud velocity dispersion of $\sim 5\,\mathrm{km\,s^{-1}}$ within each spiral arm,

while it is comparable to the typical velocity dispersion of Hɪ emission. Inspection of the Hɪ spectra (HI4PI Collaboration et al. 2016) of those clouds indeed reveals a dimmer emission peak that lies beyond the Outer arm but is not entirely separated from it (Fig. 2). These would provide natural explanations for the ignoring of the outermost feature by previous Hɪ studies.

Our observed spiral-arm loci from CO are indicated by colored lines in Fig. 1, which were derived from the average (weighted by cloud mass) of v_{lsr} of MCs in each 5° bin. While there are slight offsets between the colored and grey lines in certain regions, they can still be regarded as consistent structures. The histograms illustrate the molecular gas masses summed over 5° intervals, which are not evenly distributed along all spiral arms (Fig. 1b). For instance, the Outer arm becomes less prominent between a Galactic longitude range of $100° < l < 165°$, and the OSC arm appears dim in the range $70° < l < 100°$. Another possible reason for the scarcity of clouds in the latter region could be due to a large warp in the outskirts of our Galaxy that extends beyond our current coverage range (Fig. 1c). The phase II survey of MWISP with Galactic latitude coverage up to $b = \pm 10°$ would either confirm or reject this possibility in the near future.

3. FACE-ON VIEW OF THE OUTER GALACTIC MOLECULAR DISK

By assuming the new rotation curve and Galactic parameters from fit A5 of Reid et al. (2019), we calculated the distance for each MC and converted the heliocentric coordinates (l, b, v_{lsr}) to the Galactocentric cylindrical coordinates (R, ϕ, z). The face-on distribution of MCs in the outer Galaxy is present in Fig. 3a. Within each component, the overdense region is discernible but not very clear owing to the significant overlapping of MCs. To better indicate spiral arms, we need to reduce the map along the direction perpendicular to the disk. To reproduce a top-down view of the molecular disk, we need to project each extended cloud onto a regular x-y grid and then accumulate the emission within each cell. We assume a two-dimensional Gaussian profile for each MC (e.g., Hou et al. 2009; Hou & Han 2014).

$$L(x, y) = \sum_i \frac{W_i}{2\pi\sigma_i{}^2} exp(-\frac{(x - x_i)^2 + (y - y_i)^2}{2\sigma_i{}^2}). \quad (1)$$

Here, we adopt the measured mass of each cloud as the weight factor W_i. x_i and y_i are the coordinates of the ith MC. We choose a pixel size of 100 pc for the x-y map, which is relatively high for calculations but still somewhat larger than the typical size of the clouds. Therefore, each MC is grided with a convolution. The

convolution kernel is a Gaussian function with sigma of one-third the pixel size of the map. As a result, the standard deviation σ_i of the profile was derived from the convolution result of the size of MC and that of the convolution kernel. Note that a map derived from the central velocity of each MC can help reduce the blurring effect caused by the variation in velocities across different parts of the cloud due to turbulence or other random motions. Hence, this method allows for better visualization of the spiral structure compared to directly converting it from the velocity of each voxel in the PPV cube.

Fig. 3b is essentially a face-on surface density distribution map and the intensity is normalized to unity. Fig. 3c shows the same map as Fig. 3b, but with cloud masses corrected for variations in X_{CO} and sensitivity clipping factors (Paper ɪ). It is important to note that while these corrections improve the mass completeness for detected clouds, the incompleteness in detecting low-mass clouds has not yet been accounted for.

An exciting result is that several spectacular spiral arms become clearly visible even on the far side of the Milky Way, with a noticeable contrast between the arm and interarm densities. These CO spiral structures are traced out to a radius of ~22 kpc in the third Galactic quadrant, which is similar to that of Hɪ (Levine et al. 2006) but extends further than previous CO studies (e.g., Pohl et al. 2008; Nakanishi & Sofue 2016; Rice et al. 2016; Miville-Deschênes et al. 2017; Mertsch & Vittino 2021) by about 1.5 times. The sharper and more apparent CO spiral structure compared to Hɪ may benefit from the advantages of CO tracer with its higher angular resolution and concentration distribution along the spiral arm, as well as the method used, which minimizes the influence of smearing along the line of sight.

In Fig. 3b and Fig. 3c, the Perseus arm stands out as the most prominent structure along most of its length, appearing as a quasi-continuous spiral arm. The linear mass of arm segments, defined as the ratio of total mass to arm length, is also seems to be largest for the Perseus arm in the studied azimuthal direction. Despite being known for many years, the Outer arm is clearly visible for the first time as a molecular gas feature extending nearly 33 kpc in the outer Galaxy alone, with over 65% of its total gas mass discovered through the MWISP survey. Beyond it, the large-scale molecular gas feature is exclusively traced by the MWISP data (Table 2 of Paper ɪ). Although the dimmer OSC arm segment appears fragmented in CO emission, the OSC arm in the previously studied range still exhibits quasi-continuous Hɪ emission (Dame & Thaddeus 2011; Sun et al. 2015, 2017). Next-generation surveys with even higher reso-
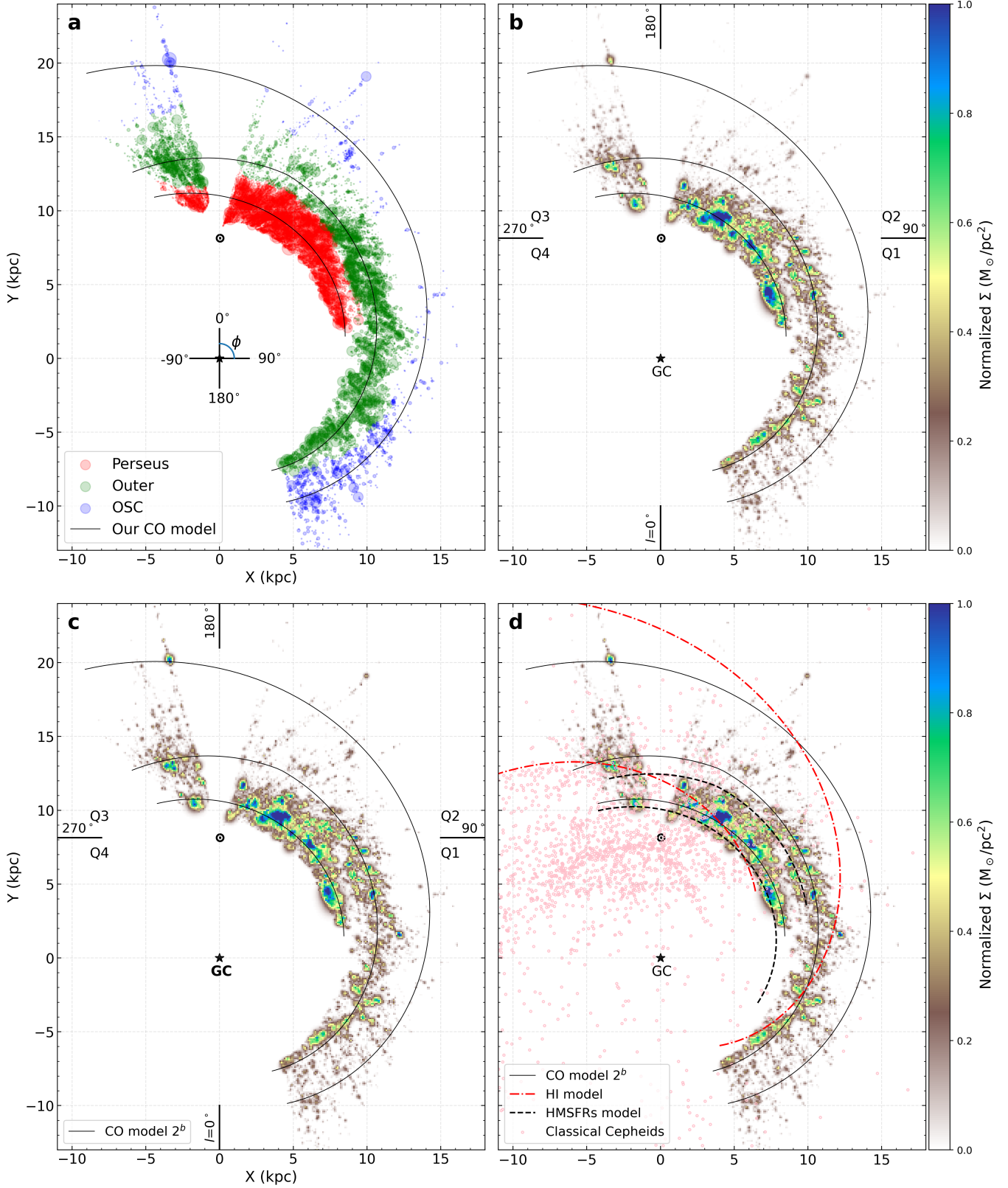
Figure 3. (*a*) Distribution of MCs projected into the Galactic plane. Each circle represents a single cloud with size scaled by cloud mass. The solid lines trace the log-periodic spiral fitting results to MCs weighted by mass. (*b*) Surface molecular gas density distribution map. Each MC was brightened with a Gaussian function. To highlight the main structure, the intensity is normalized to unity. Galactic quadrants are marked. (*c*) Same as panel (*b*), but with cloud masses corrected for variations in $X_{\rm CO}$ and sensitivity clip factors. (*d*) Comparison between CO and other tracers. Dashed lines are the models on the basis of selected HMSFRs in the Outer and Perseus arms (Reid et al. 2019). Red dot-dashed lines represent the Hi arm models (Levine et al. 2006). Pink circles indicate the classical Cepheid variable stars (Skowron et al. 2019).

lution and sensitivity can help to establish a more complete cloud catalog, thereby delineating a more continuous molecular gas distribution in this distant arm segment.

4. CO SPIRAL ARM MODEL

Following Reid et al. (2019), we attempt to fit the distribution of the MCs using a Markov chain Monte Carlo (MCMC) approach. The adopted log-periodic spiral model form can be expressed as, $\ln(R/R_{\text{kink}}) = -(\phi - \phi_{\text{kink}})\tan\psi$, where R is the Galactocentric radius, ϕ is the Galactocentric azimuth, and ψ is the pitch angle. Both uniform and abrupt changes in pitch angle on either side of the "kink" (with a radius of R_{kink} and an azimuth ϕ_{kink}) are tested. The data are variance-weighted by the cloud mass. The cloud mass derived by constant X_{CO} (termed as "model 1" in Table 1) and varied X_{CO} and sensitivity clipping factors ("model 2") are both considered. It seems that varying X_{CO} and flux clip factors only marginally affects the obtained CO spiral arm model.

We fitted the model using both the full sample (referred to as "a" in Table 1) and a subsample (termed "b" in Table 1), which excludes clouds with masses below the mean mass of MCs in the Perseus arm, as well as MCs that may have significantly large kinematic distances and regions with potentially lower completeness (see notes in Table 1). Since more massive clouds are more likely to be located within the arm regions, model "b" is expected to provide a more accurate fit. The resulting log-periodic spiral models for "b" are shown as solid lines in Fig. 3. The Outer arm can be better fitted by a model with varying pitch angles, i.e., $\psi=10.9°$ for the segment with $\phi >17.8°$ and $\psi=3.5°$ for the other segment. While a constant pitch angle of $12.3°$ fits the MCs in the current OSC arm segment, even including those in the third quadrant. This further provides support to our suggestion of the far extension of the OSC arm into the third quadrant. For the Perseus arm, excluding the second Galactic quadrant—where there is significant uncertainty in kinematic distances—allowed for a better fit of gas emissions in the first and third quadrants. The resulting pitch angle for this model is $8.8°$ (Table 1).

The geometries of the spiral arms potentially containing clues of their origin have also been extensively modeled by various tracers and methods (e.g., Binney & Tremaine 2008; Dobbs & Baba 2014). Levine et al. (2006) yielded pitch angles ranging from $21°$ to $25°$ by fitting the overdense peak of H I, which is par-

tially confirmed by the overdense maps of young upper main sequence stars, classical Cepheids, and young clusters (e.g., Poggio et al. 2021; Gaia Collaboration et al. 2023; Drimmel et al. 2024). Other tracers like high mass star-forming regions (HMSFRs) or H II regions indicated a much shallower pitch angle (e.g., Georgelin & Georgelin 1976; Taylor & Cordes 1993; Russeil et al. 2007; Reid et al. 2019; Xu et al. 2023). Although the quasi-stationary density wave theory predicts spatial displacements between different arm components (e.g., Lin & Shu 1964; Roberts 1969; Hou & Han 2015), it may not fully account for the large discrepancy reported between different tracers. Our CO models do not favor high-pitch-angle arms (Fig. 3d). It is important to note that material is not always evenly distributed along the spiral arm, which may make the dim segment even less evident in the overdense x-y map. Therefore, caution should be taken when fitting the arm model solely by connecting the overdense arm segments in the x-y map, as this may lead to an irrational connection between the segments due to uneven material distribution along the spiral arm.

Compared with the more precise parallax-based model using HMSFRs (Reid et al. 2019), we find that the two known CO spiral arms align well in shape with those traced by HMSFRs, though with slight positional offsets: approximately 0.5 kpc for the Perseus arm and about 1 kpc for the Outer arm (see Fig. 3d). These offsets may result from differences in arm tracers and uncertainties in kinematic distances. For instance, an LSR velocity uncertainty of around $5\,\text{km}\,\text{s}^{-1}$ could lead to an average kinematic distance uncertainty of about 0.47 kpc for the Perseus arm and 0.95 kpc for the Outer arm. Given these potential sources of variation, we do not address these offsets further in our analysis. We should also note that a smaller distance for the Perseus arm and Outer arm would only make the arms stand out more clearly in our analysis. Therefore, while the uncertainty of the kinematic distance may affect some details, it will not significantly alter the overall picture of the CO spiral patterns.

Figure 3d also shows a comparison with the spatial distribution of the classical Cepheids (Skowron et al. 2019), which are thought to be more numerous than young clusters (Poggio et al. 2021; Minniti et al. 2021; Gaia Collaboration et al. 2023). However, the Cepheids are still not numerous enough to well define the spiral structure, particularly on the far side of the Milky Way. In summary, while significant progress is being made for each tracer, there is still a long way to go before uncovering and fully understanding the displacements between various tracers.

Table 1. Parameters of each CO spiral arm segment derived from the MWISP data.

| Arm	ϕ range	Length	Mass	M/L	N	ϕ_{kink}	R_{kink}	$\psi_<$	$\psi_>$	Mass	M/L	N	ϕ_{kink}	R_{kink}	$\psi_<$	$\psi_>$
			Constant X_{CO}							Variations in X_{CO} & sensitivity clip factors						
					Model 1							Model 2				
	(°)	(kpc)	(M$_\odot$)	(M$_\odot$ kpc^{-1})		(°)	(kpc)	(°)	(°)	(M$_\odot$)	(M$_\odot$ kpc^{-1})		(°)	(kpc)	(°)	(°)
(1)	(2)	(3)	(4)	(5)	(6)	(7)	(8)	(9)	(10)	(11)	(12)	(13)	(14)	(15)	(16)	(17)
Perseus[a]	$-19.7\rightarrow-3.8$, $1.5\rightarrow77.4$	16.2	2.4×10^7	1.5×10^6	21,420	30.0	10.1	9.8	9.8	4.0×10^7	2.5×10^6	21,420	30.0	10.1	9.7	9.7
Perseus[b]					601	30.0	9.7	9.0	9.0			499	30.0	9.8	8.8	8.8
Outer[a]	$-26.8\rightarrow-4.7$, $6.2\rightarrow150.4$	32.9	1.6×10^7	4.9×10^5	9,436	20.3	13.3	3.5	11.1	3.3×10^7	1.0×10^6	9,436	17.1	13.5	3.2	11.1
Outer[b]					1,826	20.6	13.2	3.6	11.0			1,795	17.8	13.4	3.5	10.9
OSC[a]	$-27.3\rightarrow-8.3$, $9.6\rightarrow155.8$	43.4	1.7×10^6	3.9×10^4	1,306	47.0	16.2	12.3	12.3	4.8×10^6	1.1×10^5	1,306	47.0	16.3	12.2	12.2
OSC[b]					291	47.0	16.2	12.5	12.5			367	47.0	16.4	12.3	12.3

NOTE—Column (1): arm segment. In case "a", we rely on an unselected cloud sample for the spiral arm fitting. In case "b", those MCs with mass below the mean value of clouds' mass of the Perseus arm are excluded, specifically, with $M<1.1\times10^3$ M$_\odot$ are excluded for model 1 fit, and $M<2.8\times10^3$ M$_\odot$ are excluded for model 2 fit. The Perseus arm clouds in the second Galactic quadrant are further excluded due to their significant large uncertainty of kinematic distance (e.g., Xu et al. 2006; Peek et al. 2022). Additionally, MCs of the Perseus arm in the $\phi>72°$ are also excluded for the log-periodic spiral fitting considering the potential incompleteness of cloud sample. Column (2): ϕ range of the arm segment traced by MCs. Columns (3)-(6): total length and total mass of the arm segment traced by the MWISP data, ratio between the total mass and total length of each arm segment. Column (6): the number of MCs used to arm fitting. Columns (7)-(10): parameters from log-periodic spiral fitting that under the consumption of constant CO-to-H$_2$ conversion factor. $\psi_<$ and $\psi_>$ are pitch angles for azimuths $<\phi_{kink}$ and $\geqslant\phi_{kink}$, respectively. The case $\psi_< = \psi_>$ indicates a constant pitch angle obtained. Columns (11)-(17): same as Cols. (4)-(10) but incorporate variations of X_{CO} and sensitivity clip factors.

5. GALACTIC OUTSKIRTS

The 1306 distant MCs not only well delineate the outermost structures of our Galaxy, they serving as so far the largest cloud sample possessed low density and low metallicity, are also valuable targets for a broad range of research (e.g., Watson & Koda 2017; Méndez-Delgado et al. 2022; Koda et al. 2022; Braine et al. 2023; Fontani et al. 2024). This sample, together with ten MCs (Dame & Thaddeus 2011), 14 H II regions (Anderson et al. 2012, 2015; Armentrout et al. 2017), and seven star-forming masers (Sanna et al. 2017; Sun et al. 2018b; Armentrout et al. 2017) in the OSC arm from literature, is superposed on a recent conception of the Milky Way provided by the Bar and Spiral Structure Legacy (BeSSeL) Survey (see Fig. 4). Note that the H II regions include 12 listed in Table 6 of Armentrout et al. (2017), along with G149.746−0.199 and G195.648−0.106. The seven starforming masers are also summarized in Table 3 of Vallée (2020). The log-periodic lines with a constant pitch angle of 12° indicate the two approximately symmetrical spirals in the inner Galaxy (black line) and their continuation in the outer Galaxy (white line)–namely the Scutum-Centaurus and Perseus arms. These arms have long been assumed to be density wave arms starting at opposite ends of the Galactic bar (e.g., Drimmel 2000; Dame & Thaddeus 2008; Benjamin 2009; Churchwell et al. 2009), although convincing evidence has remained elusive (e.g., Dame & Thaddeus 2011).

Evidence for such models involves tracing spiral arms on the far side of the Galaxy due to their characteristic of long and symmetric shape (Dame & Thaddeus 2011). It was not until 2011, however, that the mirror-symmetrical counterpart of the Perseus arm was discovered, depicted by the ten distant MCs along the extension of the Scutum-Centaurus arm in the outer first quadrant (e.g., Dame & Thaddeus 2011). Adding a large number of MCs along the extension of the Scutum-Centaurus arm makes the whole arm even longer, extending over a length of $\sim$80 kpc and wrapping a full 360° around the Galaxy, though in a "looser" or less regular manner. Our findings provide some robust evidence supporting the view of symmetry density wave arms. Future high-quality data from the southern sky are called for to reveal the expected extension of the Perseus arm as the symmetric counterpart of the present new segment.
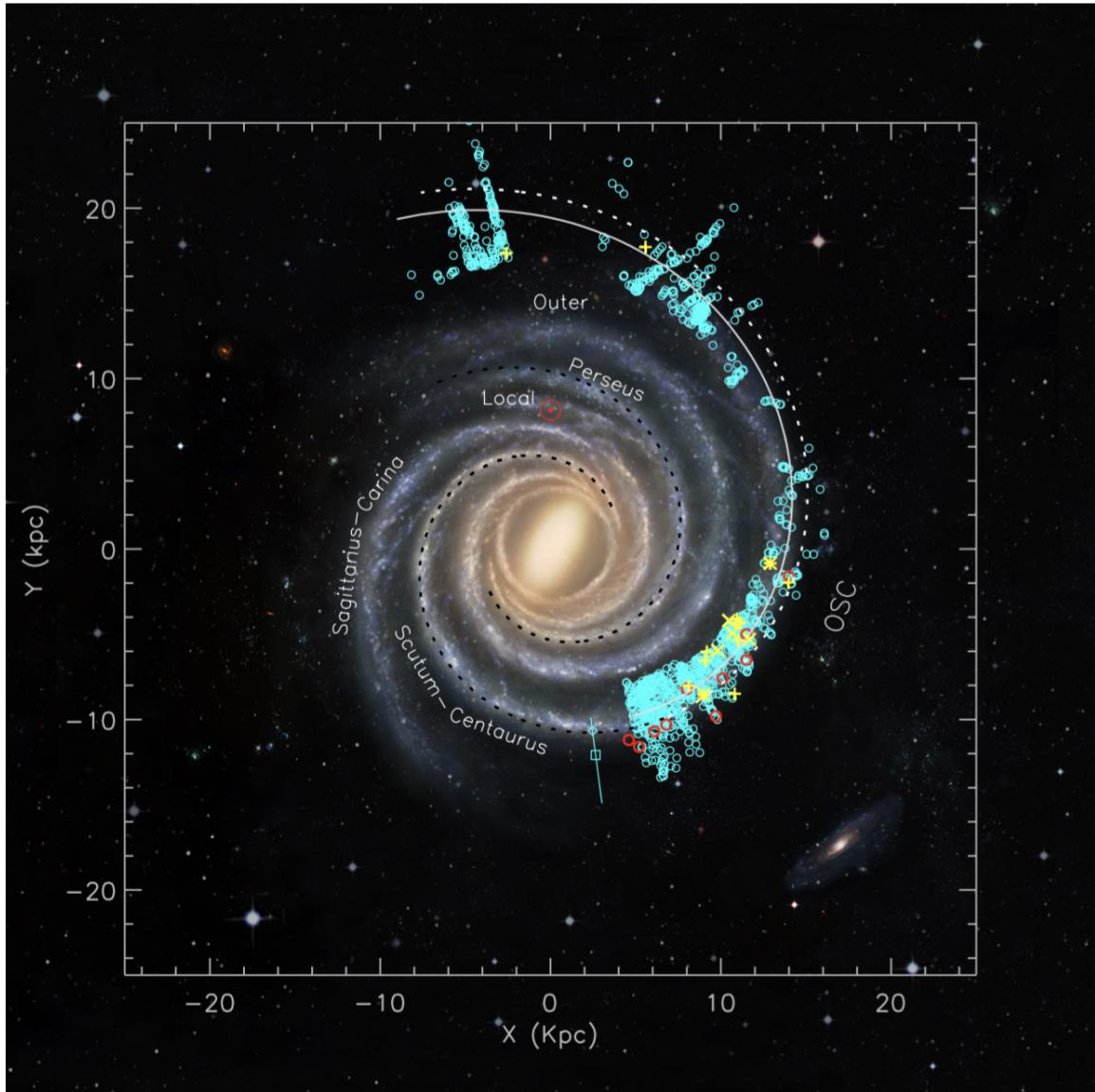
Figure 4. Molecular clouds and HMSFRs at the Galactic outskirts. The available distant MCs are superposed on the new view of the Milky Way based on 200 trigonometric parallaxes for masers in HMSFRs (credit: Xing-Wu Zheng & Mark Reid BeSSeL/NJU/CfA). The 1306 MCs from this study and 10 MCs from the literature (Dame & Thaddeus 2011) are indicated by cyan and red circles, respectively. The two symmetrical spirals and their extensions–namely the Scutum-Centaurus and Perseus arms, are indicated by two logarithmic spirals with a pitch angle of $12°$ averaged over various tracers (Vallée 2008). The solid logarithmic spiral indicates the fit for the OSC arm (CO model 2^b). The cyan square denotes the HMSFR of the OSC arm with trigonometric parallax measurement (Sanna et al. 2017). The diamond marks the location of the HMSFR calculated by the kinematic method. The yellow pluses and crosses indicate the distant HII regions (Anderson et al. 2012, 2015; Armentrout et al. 2017) and star-forming masers (Armentrout et al. 2017; Sun et al. 2018b), respectively.

Facility: PMO-13.7 m telescope

REFERENCES

Alexander, S. 1852, AJ, 2, 158

Anderson, L. D., Armentrout, W. P., Johnstone, B. M.,
et al. 2015, ApJS, 221, 26

Anderson, L. D., Bania, T. M., Balser, D. S., & Rood,
R. T. 2012, ApJ, 754, 62

Armentrout, W. P., Anderson, L. D., Balser, D. S., et al.
2017, ApJ, 841, 121

Benjamin, R. A. 2009, in The Galaxy Disk in Cosmological
Context, ed. J. Andersen, Nordströara, B. m, &
J. Bland-Hawthorn, Vol. 254, 319–322

Binney, J., & Tremaine, S. 2008, Galactic Dynamics:
Second Edition

Braine, J., & Herpin, F. 2004, Nature, 432, 369

Braine, J., Sun, Y., Shimajiri, Y., et al. 2023, A&A, 676,
A27

Burton, W. B. 1971, A&A, 10, 76

Churchwell, E., Babler, B. L., Meade, M. R., et al. 2009,
PASP, 121, 213

Dame, T. M., & Thaddeus, P. 2008, ApJL, 683, L143

—. 2011, ApJL, 734, L24

Dobbs, C., & Baba, J. 2014, PASA, 31, e035

Dong, Y., Sun, Y., Xu, Y., et al. 2023, Distributions and
Physical Properties of Molecular Clouds in the Third
Galactic Quadrant: l = [219.°75, 229.°75] and b = [-5.°25,
5.°25], , , arXiv:2308.10484

Drimmel, R. 2000, A&A, 358, L13

Drimmel, R., Khanna, S., Poggio, E., & Skowron, D. M.
2024, arXiv e-prints, arXiv:2406.09127

Du, X., Xu, Y., Yang, J., et al. 2016, ApJS, 224, 7

Ester, M., Kriegel, H.-P., Sander, J., & Xu, X. 1996, in
Second International Conference on Knowledge Discovery
and Data Mining (KDD'96). Proceedings of a conference
held August 2-4, 226–331

Fontani, F., Vermariën, G., Viti, S., et al. 2024, arXiv
e-prints, arXiv:2409.07243

Gaia Collaboration, Drimmel, R., Romero-Gómez, M.,
et al. 2023, A&A, 674, A37

Georgelin, Y. M., & Georgelin, Y. P. 1976, A&A, 49, 57

Heyer, M., & Dame, T. M. 2015, ARA&A, 53, 583

HI4PI Collaboration, Ben Bekhti, N., Flöer, L., et al. 2016,
A&A, 594, A116

Hou, L. G., & Han, J. L. 2014, A&A, 569, A125

—. 2015, MNRAS, 454, 626

Hou, L. G., Han, J. L., & Shi, W. B. 2009, A&A, 499, 473

Kalberla, P. M. W., & Kerp, J. 2009, ARA&A, 47, 27

Kerr, F. J. 1969, ARA&A, 7, 39

Kerr, F. J., Hindman, J. V., & Carpenter, M. S. 1957,
Nature, 180, 677

Koda, J., Watson, L., Combes, F., et al. 2022, ApJ, 941, 3

Koo, B.-C., Park, G., Kim, W.-T., et al. 2017, PASP, 129,
094102

Levine, E. S., Blitz, L., & Heiles, C. 2006, Science, 312, 1773

Lin, C. C., & Shu, F. H. 1964, ApJ, 140, 646

McClure-Griffiths, N. M., Stanimirović, S., & Rybarczyk, D. R. 2023, ARA&A, 61, 19

Méndez-Delgado, J. E., Amayo, A., Arellano-Córdova, K. Z., et al. 2022, MNRAS, 510, 4436

Mertsch, P., & Phan, V. H. M. 2023, A&A, 671, A54

Mertsch, P., & Vittino, A. 2021, A&A, 655, A64

Minniti, J. H., Zoccali, M., Rojas-Arriagada, A., et al. 2021, A&A, 654, A138

Miville-Deschênes, M.-A., Murray, N., & Lee, E. J. 2017, ApJ, 834, 57

Nakanishi, H., & Sofue, Y. 2016, PASJ, 68, 5

Peek, J. E. G., Tchernyshyov, K., & Miville-Deschenes, M.-A. 2022, ApJ, 925, 201

Poggio, E., Drimmel, R., Cantat-Gaudin, T., et al. 2021, A&A, 651, A104

Pohl, M., Englmaier, P., & Bissantz, N. 2008, ApJ, 677, 283

Reid, M. J., Menten, K. M., Brunthaler, A., et al. 2019, ApJ, 885, 131

Rice, T. S., Goodman, A. A., Bergin, E. A., Beaumont, C., & Dame, T. M. 2016, ApJ, 822, 52

Roberts, W. W. 1969, ApJ, 158, 123

Russeil, D., Adami, C., & Georgelin, Y. M. 2007, A&A, 470, 161

Sanna, A., Reid, M. J., Dame, T. M., Menten, K. M., & Brunthaler, A. 2017, Science, 358, 227

Shan, W., Yang, J., Shi, S., et al. 2012, IEEE Transactions on Terahertz Science and Technology, 2, 593

Skowron, D. M., Skowron, J., Mróz, P., et al. 2019, Science, 365, 478

Strasser, S. T., Dickey, J. M., Taylor, A. R., et al. 2007, AJ, 134, 2252

Su, Y., Sun, Y., Li, C., et al. 2016, ApJ, 828, 59

Su, Y., Yang, J., Zhang, S., et al. 2019, ApJS, 240, 9

Sun, J. X., Lu, D. R., Yang, J., et al. 2018a, Acta Astronomica Sinica, 59, 3

Sun, Y., Su, Y., Zhang, S.-B., et al. 2017, ApJS, 230, 17

Sun, Y., Xu, Y., Yang, J., et al. 2015, ApJL, 798, L27

Sun, Y., Xu, Y., Chen, X., et al. 2018b, ApJ, 869, 148

Sun, Y., Yang, J., Yan, Q.-Z., et al. 2021, ApJS, 256, 32

Taylor, J. H., & Cordes, J. M. 1993, ApJ, 411, 674

Vallée, J. P. 2008, AJ, 135, 1301

—. 2020, ApJ, 896, 19

Watson, L. C., & Koda, J. 2017, in Astrophysics and Space Science Library, Vol. 434, Outskirts of Galaxies, ed. J. H. Knapen, J. C. Lee, & A. Gil de Paz, 175

Weaver, H. 1974, in IAU Symposium, Vol. 60, Galactic Radio Astronomy, ed. F. J. Kerr & S. C. Simonson, 573

Xu, Y., Hao, C. J., Liu, D. J., et al. 2023, ApJ, 947, 54

Xu, Y., Hou, L.-G., & Wu, Y.-W. 2018, Research in Astronomy and Astrophysics, 18, 146

Xu, Y., Reid, M. J., Zheng, X. W., & Menten, K. M. 2006, Science, 311, 54

Yan, Q.-Z., Yang, J., Su, Y., Sun, Y., & Wang, C. 2020, ApJ, 898, 80

Yan, Q.-Z., Yang, J., Su, Y., et al. 2022, AJ, 164, 55

Yang, J., Shan, W., Shi, S., et al. 2008, in 2008 Global Symposium on Millimeter Waves, IEEE, 177–179